Materials Transactions, Vol. 43, No. 8 (2002) pp. 2137 to 2142

Effects of Chromium on the Glass Formation and Corrosion Behavior of Bulk Glassy Fe–Cr–Mo–C–B Alloys

Shujie Pang, Tao Zhang, Katsuhiko Asami and Akihisa Inoue

Institute for Materials Research, Tohoku University, Sendai 980-8577, Japan

Bulk glassy $Fe_{60-x}Cr_xMo_{15}C_{15}B_{10}$ ($x = 0$, 7.5, 15, 22.5 and 30 at%) alloys with high thermal stability were synthesized and the effects of chromium on the glass formation and corrosion behavior were clarified. The maximum diameter for glass formation is 2–2.5 mm for the 7.5 and 15 at%Cr alloys and 1 mm for the other alloys. In the present glassy alloy system, the temperature interval of the supercooled liquid region (ΔT_x) changed with chromium and was enlarged from around 70 K at $x = 0$, 22.5 and 30 at% to over 80 K at $x = 7.5$ and 15 at%. Both corrosion rate and anodic current density by potentiodynamic polarization in HCl solutions decreased with an increase of chromium content in the alloys. For the Cr-free alloy, molybdenum was significantly concentrated in the surface film after immersion in 1 N HCl solution. The bulk glassy alloys containing chromium was immune to corrosion by the formation of protective passive film enriched with chromium during immersion in the solution.

(Received May 14, 2002; Accepted June 17, 2002)

Keywords: *bulk glassy alloy, iron-based alloy, chromium, supercooled liquid, corrosion, X-ray photoelectron spectroscopy (XPS), passive film*

1. Introduction

Glassy alloys are attractive for synthesizing new alloys with high corrosion resistance because of the formation of a single solid solution phase exceeding the solubility limits of alloying elements in the equilibrium state and hence allowing selective alloying of strongly passivating elements. It is known that a number of Fe-based glassy alloys with high corrosion resistance in aggressive media have been fabricated.[1,2] However, they have mainly been fabricated as sputtered thin films and melt-spun ribbons because of their low glass-forming ability (GFA). The small size and low thermal stability of the Fe-based glassy alloys has prevented the further extension of their application fields as corrosion resistant materials. Recently, the $Fe_{43}Cr_{16}Mo_{16}(C, B, P)_{25}$ bulk glasses with thickness up to about 2.5 mm have been formed by a conventional copper-mold casting method.[3] These bulk glassy alloys exhibited a glass transition, followed by a large supercooled liquid region before crystallization. As is the case for the La–Al–TM,[4] Zr–Al–TM,[5–7] Fe–(Al, Ga)–(P, C, B, Si, Ge),[8,9] Fe–(Co, Ni)–(Zr, Nb, Ta)–B,[10] Fe–C–Si–B,[11,12] Fe–Co–Ni–Si–B,[13] Pd–Cu–Ni–P,[14] Ti–Cu–Ni–B–Sn–Si,[15] Co–Fe–Nb–Zr–B,[16] Cu–Zr–Ti–Y,[17] Cu–Zr–Ti[18] and Cu–Hf–Ti[18] (TM = transition metal) bulk glassy alloys developed during the last decade, the Fe–Cr–Mo–C–B–P system alloys satisfy the following three empirical rules[19] for the achievement of high GFA, *i.e.*, 1) multicomponent alloy systems consisting of more than three elements, 2) significant atomic size mismatches above 12% among the main elements, and 3) suitable negative heats of mixing among the main constituent elements. It is well known that chromium is one of the most effective elements for improving the corrosion resistance of Fe-based alloys in aggressive acids with low oxidizing ability. On the other hand, the change of chromium content in alloys is also expected to influence the GFA of the alloys. Therefore, this work aims to present the effects of chromium on the glass formation and corrosion behavior for $Fe_{60-x}Cr_xMo_{15}C_{15}B_{10}$ alloys. The origin for the effects of chromium is also discussed.

2. Experimental

Multicomponent alloys with nominal compositions of $Fe_{60-x}Cr_xMo_{15}C_{15}B_{10}$ (at%) were examined in the present work. Alloy ingots were prepared from mixtures of pure Fe, Cr, Mo, C and B as well as pre-alloyed Fe–C alloy by induction melting in an argon atmosphere. From the master alloy ingots, bulk specimens in a rod shape of about 40 mm in length were prepared by copper mold casting. Ribbon samples with a thickness of about 20 μm and a width of about 1 mm were fabricated by single-roller melt spinning.

The structure of the rapidly solidified specimens was examined by X-ray diffraction using Cu–Kα radiation. The thermal stability associated with glass transition, supercooled liquid and crystallization for the glassy alloys was investigated by differential scanning calorimetry (DSC) at a heating rate of 0.67 K/s. The liquidus temperatures of the alloys were measured by differential thermal analysis (DTA) at a heating rate of 0.33 K/s.

Corrosion behavior of the bulk glassy alloys was evaluated by weight loss and electrochemical polarization measurements. Prior to the immersion test and electrochemical measurements, the specimens were mechanically polished in cyclohexane with silicon carbide paper up to No. 1500, degreased in acetone, washed in distilled water, dried in air and further exposed to air for 24 h for good reproducibility. Electrolytes used were 1, 6 and 12 N HCl solutions prepared from reagent grade chemical and distilled water. The corrosion rates were estimated from the weight loss of the bulk glassy alloys after immersion in HCl solutions open to air at 298 K for 168 h (one week). The electrochemical measurements were conducted in a three-electrode cell using a platinum counter electrode and a Ag/AgCl reference electrode. Anodic polarization curves were measured potentiodynami-

cally with a potential sweep rate of 50 mV/min in the HCl solutions after immersing the specimens in the solutions for 20 min, when the open-circuit potentials (E_{corr}) became almost steady.

For surface analysis of the bulk glasses exposed to air for 24 h after mechanical polishing and those immersed in the HCl solutions for 168 h, X-ray photoelectron spectroscopy (XPS) measurements were performed by using a photoelectron spectrometer with Al–Kα excitation ($h\nu = 1486.6$ eV). The composition and thickness of the surface film and the composition of the underlying alloy surface just below the surface film were determined quantitatively by a previously proposed method.[20,21] The quantitative determination was performed under the assumption of a three-layer model of outermost contaminant hydrocarbon layer of uniform thickness, surface film of uniform thickness and underlying alloy surface of X-ray photo-electron spectroscopically infinite thickness, along with the assumption of a homogeneous distribution of constituents in each layer. The binding energies of electrons were calibrated by using the method described elsewhere.[22,23]

3. Results and Discussion

3.1 Effect of chromium on glass formation

Bulk alloys with diameters of 1–2.5 mm consisting of a glassy single phase without crystallinity were formed in the composition range of 0–30 at%Cr for the $Fe_{60-x}Cr_xMo_{15}C_{15}B_{10}$ alloys. The maximum diameter for glass formation was 1 mm for the alloys containing 0, 22.5 and 30 at%Cr, 2 mm for the 7.5 at%Cr alloy and 2.5 mm for the 15 at%Cr alloy, respectively. The DSC curves of the bulk glassy alloys shown in Fig. 1 exhibit a sequential transition of glass transition and supercooled liquid region before crystallization, where T_g and T_x are glass transition temperature and crystallization temperature, respectively. The high thermal stability of the supercooled liquid is indicated by the large temperature interval of supercooled liquid region ($\Delta T_x = T_g - T_x$) exceeding 70 K. The glassy single phase of the bulk samples was further confirmed by comparing their DSC curves with those of the melt-spun ribbons. Figure 2 shows the DSC curves of the glassy $Fe_{45}Cr_{15}Mo_{15}C_{15}B_{10}$ melt-spun ribbon and cast rod with a diameter of 2.5 mm, where the heat of the main crystallization reaction is 4.73 kJ/mol and 4.71 kJ/mol for the glassy ribbon and rod samples, respectively. It is indicated that there is no distinct difference in the T_g, T_x and heat of crystallization between the bulk and ribbon samples.

The formation of the bulk Fe–(Cr–)Mo–C–B glasses is attributed to the satisfaction of the three empirical rules[19] for the achievement of high GFA and the stabilization of the supercooled liquid. The atomic size ratios for TM/metalloid (TM = Fe, Cr and Mo) in the present system are 0.57–0.73.[24] The heats of mixing are negative values of 1–19 kJ/mol for the atomic pairs of TM–B, Fe–Cr and Fe–Mo.[25] Thus, the data on the atomic size and the chemical bonding nature indicate that the present Fe–(Cr–)Mo–C–B alloys satisfy the three empirical rules. The satisfaction is favorable for the formation of a glassy structure with the features of highly dense random packed atomic configurations, new local atomic configurations and long-range homogeneous atomic configurations with attractive interactions. The formation of such a structure leads to the suppression of nucleation and growth reactions of a crystalline phase, a high viscosity and a lower atomic diffusivity. Therefore, the $Fe_{60-x}Cr_xMo_{15}C_{15}B_{10}$ alloys with the low nucleation and growth reactions and low atomic diffusivity can have high GFA leading to the formation of the bulk glasses.

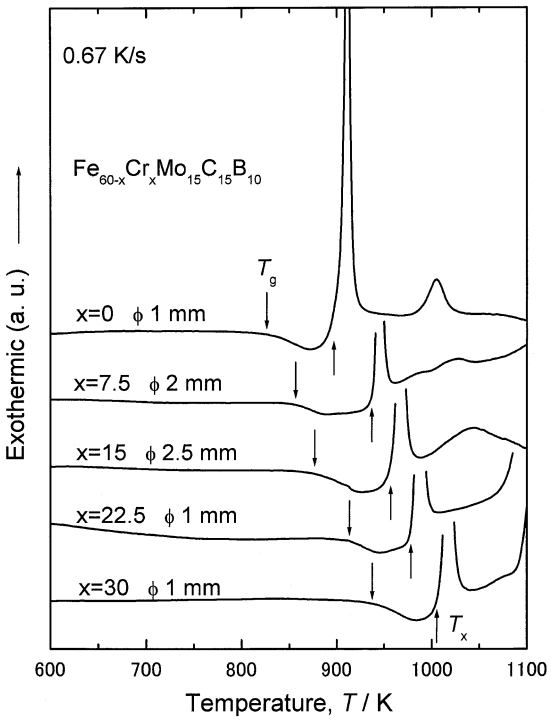

Fig. 1 DSC curves of the bulk glassy $Fe_{60-x}Cr_xMo_{15}C_{15}B_{10}$ alloys with their maximum diameters for glass formation.

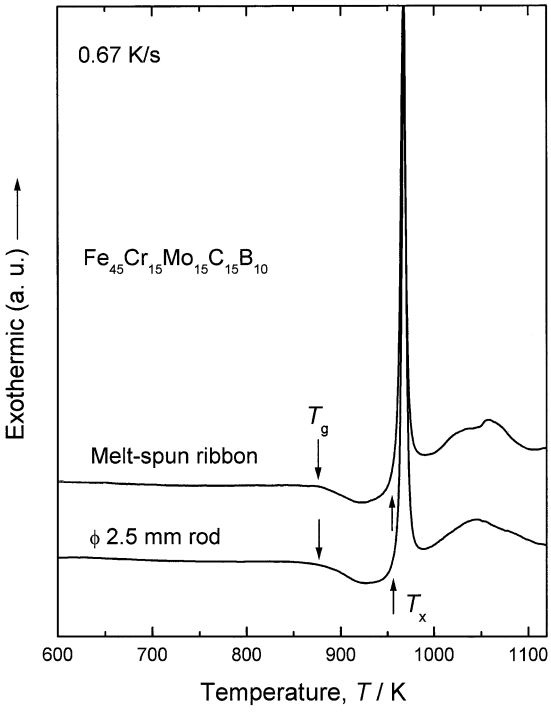

Fig. 2 DSC curves of the glassy $Fe_{45}Cr_{15}Mo_{15}C_{15}B_{10}$ melt-spun ribbon and cast rod with a diameter of 2.5 mm.

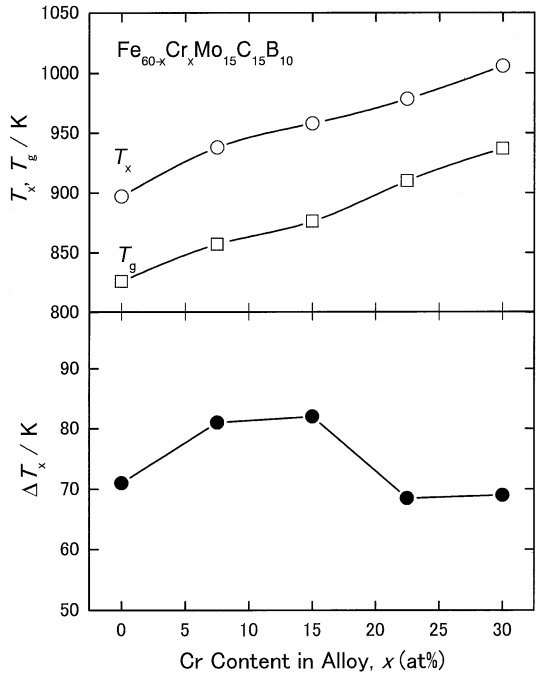

Fig. 3 Changes in T_g, T_x and ΔT_x with chromium content for the bulk glassy $Fe_{60-x}Cr_xMo_{15}C_{15}B_{10}$ alloys.

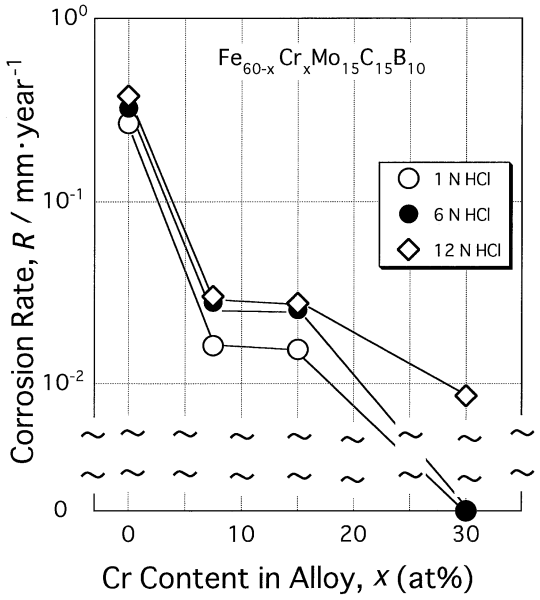

Fig. 4 Corrosion rates of the bulk glassy $Fe_{60-x}Cr_xMo_{15}C_{15}B_{10}$ alloys in HCl solutions plotted versus chromium content.

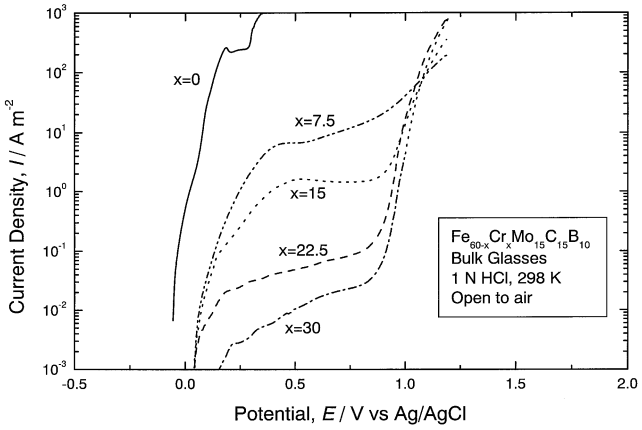

Fig. 5 Anodic polarization curves of the bulk glassy $Fe_{60-x}Cr_xMo_{15}C_{15}B_{10}$ alloys with their maximum diameters for glass formation in 1 N HCl solution open to air at 298 K.

For the present alloy system, it is noticed that the maximum diameter for glass formation changes with chromium content, indicating that chromium content in the alloys has an appreciable effect on the GFA. It is generally known that the main factors for high GFA are a high reduced glass transition temperature (T_g/T_l, where T_l is liquidus temperature) and a large temperature interval of supercooled liquid region (ΔT_x). It was found that the T_g/T_l, which was determined by the T_g on the DSC curves and the T_l measured by DTA, was independent of chromium content and kept at a constant value of about 0.6 in the composition range of 0–30 at%Cr for the present alloys. Figure 3 shows the changes in T_g, T_x and ΔT_x with chromium content for the bulk glassy $Fe_{60-x}Cr_xMo_{15}C_{15}B_{10}$ alloys. It is noticed that the T_x exhibits a relatively significant increase in the composition range of 0–15 at%Cr while the T_g increases almost linearly with an increase of chromium content. As a result, the ΔT_x defined by the difference between T_g and T_x reaches relatively large values of exceeding 80 K at the chromium contents of 7.5 and 15 at%, at which the bulk glasses with diameters of 2–2.5 mm can be prepared. The change in ΔT_x versus chromium content is in agreement with that of the maximum diameters for glass formation for the $Fe_{60-x}Cr_xMo_{15}C_{15}B_{10}$ alloys as described above. Therefore, it is suggested that ΔT_x is a dominant factor for the GFA of the present alloys with different chromium contents.

3.2 Effect of chromium on corrosion behavior

Corrosion rates of the bulk glassy $Fe_{60-x}Cr_xMo_{15}C_{15}B_{10}$ alloys in HCl solutions open to air at 298 K are plotted as a function of chromium content in Fig. 4. In 1, 6 and 12 N HCl solutions, the corrosion rates of the Cr-free alloy are about 0.5 mm/year. With the addition of chromium to the alloys, the corrosion rates in all the solutions decrease significantly and are lower than 5×10^{-2} mm/year in the Cr content range above 7.5 at%. Especially the corrosion rate of the 30 at%Cr alloy is of the order of 10^{-3} mm/year even in the extremely aggressive 12 N solution and no weight loss is detected after the one-week immersion test in 1 and 6 N HCl solutions. It is indicated that the addition of chromium for replacing some portion of iron is effective for suppressing the corrosion of the glassy $Fe_{60-x}Cr_xMo_{15}C_{15}B_{10}$ alloys during open-circuit immersion in the aggressive acids.

The corrosion behavior of the bulk glassy $Fe_{60-x}Cr_xMo_{15}C_{15}B_{10}$ alloys was also examined by the potentiodynamic polarization measurement. Figure 5 shows their anodic polarization curves in 1 N HCl solution open to air at 298 K. The glassy Fe–Mo–C–B alloy suffers general corrosion by slight anodic polarization. However, the glassy Fe–Cr–Mo–C–B alloys are spontaneously passivated with large passive regions until the transpassive dissolution of chromium occurs. It is also noticed that, with an increase of chromium content in the alloys, the anodic current density decreases significantly. In 6 N HCl solution, the alloys containing 15–30 at% chromium exhibit spontaneous passivity, although their passive current

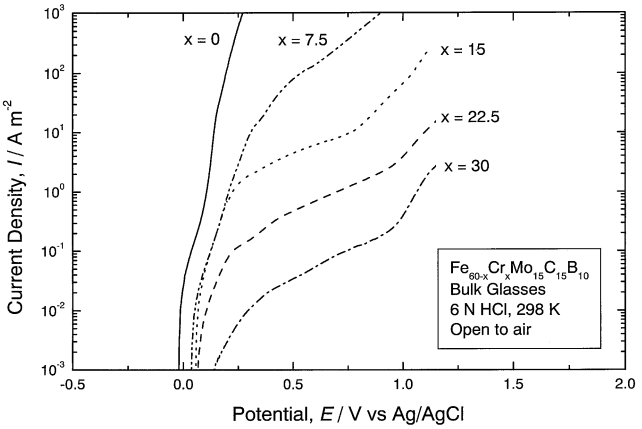

Fig. 6 Anodic polarization curves of the bulk glassy $Fe_{60-x}Cr_xMo_{15}C_{15}B_{10}$ alloys with their maximum diameters for glass formation in 6 N HCl solution open to air at 298 K.

density increases quickly with polarization resulted from the instability of their surface films by anodic polarization, as shown in Fig. 6. In 12 N HCl solution, although anodic current density of the glassy alloys increased rapidly with potential caused by the low stability of the surface films, no pitting corrosion was recognized for the alloys polarized up to 1.2 V vs. Ag/AgCl. Accordingly, it is clarified that the addition of chromium for replacing some portion of iron is effective on enhancing the corrosion resistance of the glassy Fe–Cr–Mo–C–B alloys.

For a better understanding of the effect of chromium on the corrosion resistance for the glassy $Fe_{60-x}Cr_xMo_{15}C_{15}B_{10}$ alloys, X-ray photoelectron spectroscopic analysis (XPS) was performed for the specimens exposed to air after mechanical polishing and those immersed in 1 N HCl at 298 K for 168 h. The XPS spectra over a wide binding energy region apparently exhibited peaks of carbon, oxygen, boron, iron, chromium and molybdenum. The C 1s peaks were those from carbon in alloy and so-called contaminant carbon on the top surface of the specimen. The O 1s spectrum consisted of peaks originated from oxygen in metal-O-metal bond, metal-OH bond and/or bound water. The peaks of Fe 2p, Cr 2p, Mo 3d and B 1s were composed of peaks corresponding to the species in the oxidized states in a surface film and the metallic states in an underlying alloy surface.

Figure 7 shows the Mo 3d spectrum measured from the glassy $Fe_{60}Mo_{15}C_{15}B_{10}$ and $Fe_{30}Cr_{30}Mo_{15}C_{15}B_{10}$ alloys after the immersion in 1 N HCl solution for 168 h. For the Cr-free alloy, the Mo 3d spectrum consists of Mo species in Mo^{4+}, Mo^{5+} and Mo^{6+} states and no metallic peak is detected as shown in Fig. 7(a). In addition, no peak corresponding to Fe^0 or B^0 states was detected on the spectra of Fe 2p and B 1s for the $Fe_{60}Mo_{15}C_{15}B_{10}$ alloy after the immersion. Accordingly, it is indicated that the oxidized surface film formed on the 0 at%Cr alloy after the immersion was thick and the underlying alloy surface could not be detected by XPS. By deconvoluting the Mo spectrum in Fig. 7(a) into individual peaks, it is found that about 56% of the oxidized molybdenum in the surface film is hexavalent for the $Fe_{60}Mo_{15}C_{15}B_{10}$ alloy after the immersion in 1 N HCl solution. As shown in Fig. 7(b), the Mo 3d spectrum for the glassy alloy containing 30 at% chromium is composed of peaks corresponding to four states,

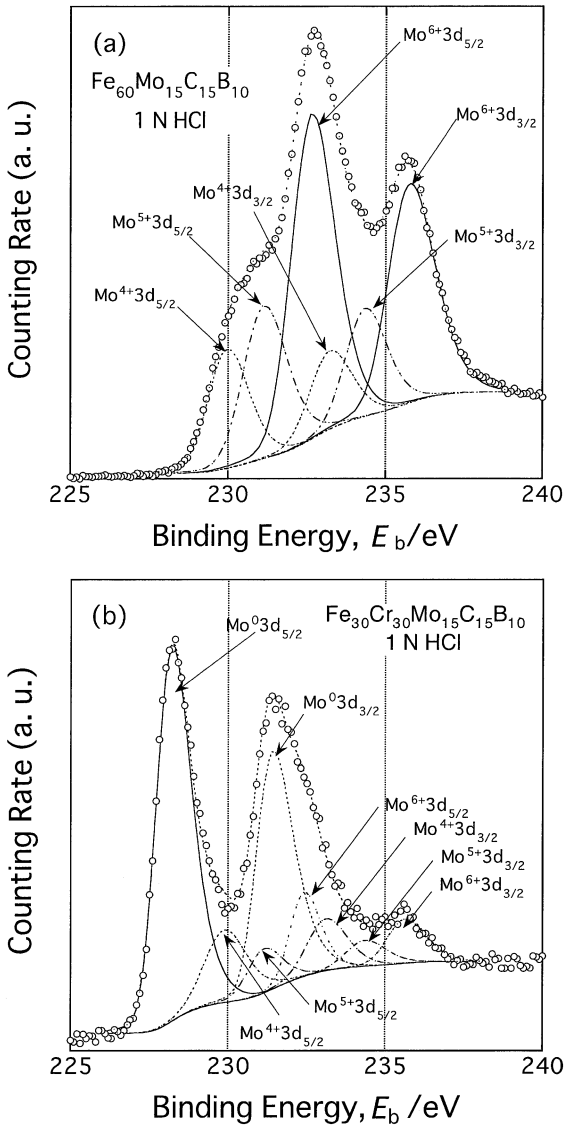

Fig. 7 Mo 3d XPS peaks of the (a) $Fe_{60}Mo_{15}C_{15}B_{10}$ and (b) $Fe_{30}Cr_{30}Mo_{15}C_{15}B_{10}$ bulk glassy alloys with a diameter of 1 mm after immersion in 1 N HCl solution at 298 K for 168 h.

i.e., a pair of metallic Mo^0 state and three doublets of Mo^{4+}, Mo^{5+} and Mo^{6+} state peaks. The peaks of the Mo species in metallic state are the most intense. Similarly, clear peaks of iron, chromium and boron species in their metallic states were found. The alloys containing chromium can possess high corrosion resistance in the solution and result in a thin surface film. The thickness of the surface films was 1.8 nm and 2.3 nm for the $Fe_{30}Cr_{30}Mo_{15}C_{15}B_{10}$ alloy before and after immersion in 1 N HCl solution, respectively. This is in agreement with the previous results that the thickness of chromium-enriched passive film is generally around 2–3 nm.[2,26,27]

Figure 8 shows the fraction of the transition metals (TM), *i.e.*, Fe, Cr and Mo in the surface films and underlying alloy surfaces for the glassy $Fe_{60}Mo_{15}C_{15}B_{10}$ and $Fe_{30}Cr_{30}Mo_{15}C_{15}B_{10}$ alloys exposed to air and those immersed in 1 N HCl solution, where ox and m represent oxidized and metallic states, respectively.

As seen in Fig. 8(a), the ratio of the fractions of iron and molybdenum in the underlying alloy surface of the $Fe_{60}Mo_{15}C_{15}B_{10}$ alloy is almost the same as their nominal

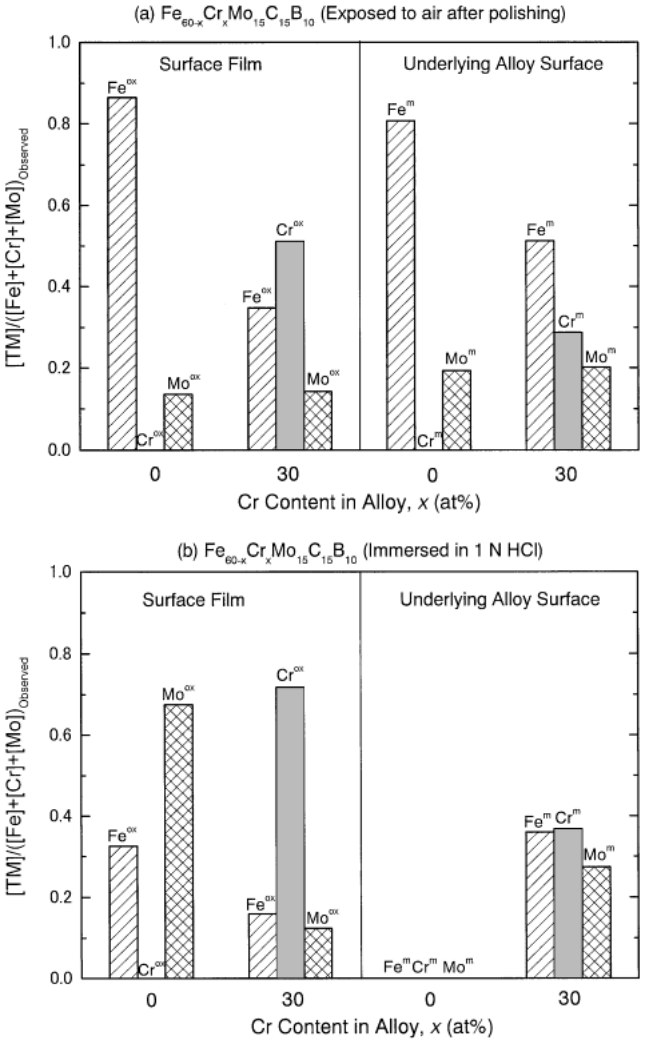

Fig. 8 Fractions of the transition metals (TM = Fe, Cr or Mo) in the surface films and the underlying alloy surfaces for the bulk glassy $Fe_{60-x}Cr_xMo_{15}C_{15}B_{10}$ ($x = 0$ and 30 at%) alloys (a) exposed to air after mechanical polishing and (b) immersed in 1 N HCl solution at 298 K for 168 h.

ratio (Fe : Mo = 80 : 20). In the surface film, the concentration of iron is slightly increased and molybdenum is depleted. On the $Fe_{30}Cr_{30}Mo_{15}C_{15}B_{10}$ alloy (the nominal ration is Fe : Cr : Mo = 40 : 40 : 20), chromium is preferentially oxidized and is depleted in the underlying alloy surface while it is enriched in the oxide film, but the ratio of Fe to Mo is not changed.

After the immersion in 1 N HCl solution for 168 h, the formation of significantly molybdenum-enriched surface film on the glassy $Fe_{60}Mo_{15}C_{15}B_{10}$ alloy is observed as shown in Fig. 8(b). As mentioned above, high concentration of the oxidized molybdenum in the surface film was hexavalent. In addition, because the surface film was significantly thick, the underlying alloy surface was undetectable by XPS. In general, a thick surface film is formed when the alloy is not resistant to the environment. On the other hand, for the alloy containing chromium, chromium is extremely enriched in the passive film and its concentration is apparently higher than that in the air-formed surface film, leading to the high immunity to corrosion in HCl solutions. On the underlying alloy surface, it is also seen that molybdenum is enriched. Considering the very low corrosion rate of the 30 at%Cr alloy in 1 N HCl solution, the chromium-enriched passive film may well be formed by the preferential dissolution of iron from the air-formed film and the reconstruction of the passive film. But judging from the comparison between the compositions before and after immersion, the underlying alloy must have dissolved to some extent at the same time.

The ratio of hexavalent Mo to the total of the oxidized Mo in the surface film on the $Fe_{30}Cr_{30}Mo_{15}C_{15}B_{10}$ alloy after the immersion was about 36%. The corrosion potential of the Fe–Mo–C–B alloy is lower than that of the Fe–Cr–Mo–C–B alloy in 1 N HCl, as seen in Fig. 5. It is often observed by XPS that Mo-containing alloys show the existence of Mo^{6+} in the potential region where thermodynamically Mo^{6+} is not formed. It is suggested that the hexavalent molybdenum is formed by air oxidation of Mo^{4+} during the transfer of the specimen from the electrolyte to the XPS apparatus through air.[2,28] Especially, a low protective surface film formed at a low potential shows high concentration of Mo^{6+}.[2,28]

The content of B in the surface films formed after the immersion was less than that in the bulk alloys. It was reported that, for Fe–Cr-metalloid amorphous alloys, addition of B was detrimental to corrosion resistance because B impeded the enrichment of Cr.[29] However, it was also found that for the $Fe_{50-x}Cr_{16}Mo_{16}C_{18}B_x$ glassy alloys, the enrichment of Cr increased with an increase in B in the alloy, while the B content in the surface films decreased relatively to its bulk compositions.[30] More investigation is necessary for clarifying the effect of addition of B.

4. Conclusions

(1) $Fe_{60-x}Cr_xMo_{15}C_{15}B_{10}$ ($x = 0$, 7.5, 15, 22.5 and 30 at%) alloys were prepared in a bulk glassy form with diameters up to 2.5 mm by copper mold casting. The maximum diameter for glass formation was 2–2.5 mm for the alloys containing 7.5 and 15 at% chromium and 1 mm for the other alloys. In the present glassy alloy system, the temperature interval of the supercooled liquid region (ΔT_x) changed with chromium content and was enlarged from around 70 K at $x = 0$, 22.5 and 30 at% to over 80 K at $x = 7.5$ and 15 at%.

(2) The addition of chromium to the glassy Fe-based alloys for replacing some portion of iron is effective for enhancing the corrosion resistance in HCl solutions. The corrosion rates of the bulk glassy alloy in 1–12 N HCl solutions are lowered from 0.5 mm/year to less than 5×10^{-2} mm/year by the addition of 7.5 at% or more chromium and down to 10^{-3} mm/year range for the 30 at%Cr alloy. Anodic current density by potentiodynamic polarization in the media decreases significantly with an increase of chromium content in the alloys.

(3) After immersion in 1 N HCl solution, molybdenum is significantly concentrated in the surface film on the Fe–Mo–C–B glassy alloy and chromium is enriched extremely in the surface films on the Fe–Cr–Mo–C–B glassy alloys. The high corrosion resistance of the bulk glassy Cr-containing alloys is originated from the formation of chromium-enriched surface film by immersion in HCl solutions.

REFERENCES

1) M. Naka, K. Hashimoto and T. Masumoto: J. Japan Inst. Metals **38** (1974) 835–841.
2) K. Asami, M. Naka, K. Hashimoto and T. Masumoto: J. Electrochem. Soc. **127** (1980) 2130–2137.
3) S. J. Pang, T. Zhang, K. Asami and A. Inoue: Acta Mater. **50** (2002) 489–497.
4) A. Inoue, T. Zhang and T. Masumoto: Mater. Trans., JIM **30** (1989) 965–972.
5) A. Inoue, T. Zhang and T. Masumoto: Mater. Trans., JIM **31** (1990) 177–183.
6) T. Zhang, A. Inoue and T. Masumoto: Mater. Trans., JIM **32** (1991) 1005–1010.
7) A. Inoue and T. Zhang: Mater. Trans., JIM **36** (1995) 1184–1187.
8) A. Inoue and J. S. Gook: Mater. Trans., JIM **36** (1995) 1180–1183.
9) A. Inoue, Y. Shinobara and G. S. Gook: Mater. Trans., JIM **36** (1995) 1427–1433.
10) A. Inoue, T. Zhang and A. Takeuchi: Appl. Phys. Lett. **71** (1997) 464–466.
11) A. Inoue and X. M. Wang: Acta Mater. **48** (2000) 1383–1395.
12) X. M. Wang and A. Inoue: Mater. Sci. Eng. **A304–306** (2001) 710–715.
13) T. Zhang and A. Inoue: Mater. Trans. **42** (2001) 1015–1018.
14) A. Inoue, N. Nishiyama and H. M. Kimura: Mater. Trans., JIM **38** (1997) 179–183.
15) T. Zhang and A. Inoue: Mater. Sci. Eng. **A304–306** (2001) 771–774.
16) T. Itoi and A. Inoue: Mater. Trans., JIM **41** (2000) 1256–1262.
17) T. Zhang, K. Kurosaka and A. Inoue: Mater. Trans. **42** (2001) 2042–2045.
18) A. Inoue, W. Zhang, T. Zhang and K. Kurosaka: Acta Mater. **49** (2001) 2645–2652.
19) A. Inoue: Mater. Trans., JIM **36** (1995) 866–875.
20) K. Asami, K. Hashimoto and S. Shimodaira: Corros. Sci. **17** (1977) 713–723.
21) K. Asami and K. Hashimoto: Corros. Sci. **24** (1984) 83–97.
22) K. Asami: J. Electron Spectrosc. Relat. Phenom. **9** (1976) 469–478.
23) K. Asami and K. Hashimoto: Corros. Sci. **17** (1977) 559–570.
24) *Metals Databook*, ed. by Japan Inst. Metals, Maruzen, Tokyo (1993) pp. 1–8.
25) F. R. de Boer, R. Boom, W. C. M. Mattens, A. R. Miedema and A. K. Niessen: *Cohesion in Metals*, (North-Holland, Amsterdam, 1989) pp. 103–637.
26) K. Hashimoto, K. Asami, M. Naka and T. Masumoto: Boshoku Gijutsu **28** (1979) 271–277.
27) H. Katagiri, S. Meguro, M. Yamasaki, H. Habazaki, T. Sato, A. Kawashima, K. Asami and K. Hashimoto: Corros. Sci. **43** (2001) 171–182.
28) M. W. Tan, E. Akiyama, A. Kawashima, K. Asami and K. Hashimoto: Corros. Sci. **38** (1996) 349–365.
29) K. Hashimoto, K. Asami, M. Naka and T. Masumoto: Boshoku Gijutsu **27** (1978) 279–283.
30) S. J. Pang, T. Zhang, K. Asami and A. Inoue: Corros. Sci. **44** (2002) 1847–1856.